

 Open access • Posted Content • DOI:10.1101/483511

Evolution of the HIV-1 RRE during natural infection reveals nucleotide changes that correlate with altered structure and increased activity over time — [Source link](#)

Chringma Sherpa, Patrick E. H. Jackson, Laurie R. Gray, Kathryn Anastos ...+3 more authors

Institutions: National Institutes of Health, University of Virginia, Albert Einstein College of Medicine

Published on: 04 Dec 2018 - bioRxiv (Urban und Fischer Verlag GmbH und Co. KG)

Related papers:

- [Single-Nucleotide Changes in the HIV Rev-Response Element Mediate Resistance to Compounds That Inhibit Rev Function](#)
- [Selection and characterization of human immunodeficiency virus type 1 mutants that are resistant to inhibition by the transdominant negative RevM10 protein.](#)
- [A Rev-Independent Human Immunodeficiency Virus Type 1 \(HIV-1\)-Based Vector That Exploits a Codon-Optimized HIV-1 gag-pol Gene](#)
- [Infection of HIV-1 To Establish Latent Element of the HIV-1 Promoter Controls the An AP-1 Binding Site in the Enhancer/Core](#)
- [Biological Characterization of Rev Variation in Equine Infectious Anemia Virus](#)

Share this paper:    

View more about this paper here: <https://typeset.io/papers/evolution-of-the-hiv-1-rre-during-natural-infection-reveals-2u2964esbe>

1 Evolution of the HIV-1 RRE during natural infection reveals nucleotide changes that
2 correlate with altered structure and increased activity over time.

3

4 Chringma Sherpa^{a*}, Patrick E. H. Jackson^{b,c*}, Laurie R. Gray^{c,d}, Kathryn Anastos^e,
5 Stuart F. J. Le Grice^{a#}, Marie-Louise Hammarskjold^{c,d}, David Rekosh^{c,d#}

6

7 ^aBasic Research Laboratory, Center for Cancer Research, National Cancer Institute,
8 National Institute of Health, Frederick, Maryland, USA

9

10 ^bDivision of Infectious Diseases and International Health, Department of Medicine,
11 University of Virginia, Charlottesville, Virginia, USA

12

13 ^cMyles H. Thaler Center for HIV and Human Retrovirus Research, University of Virginia,
14 Charlottesville, Virginia, USA

15

16 ^dDepartment of Microbiology, Immunology and Cancer Biology, University of Virginia,
17 Charlottesville, Virginia, USA

18

19 ^eAlbert Einstein College of Medicine and Montefiore Medical Center, Department of
20 Medicine, Bronx, New York, USA

21

22 Running Head: HIV-1 RRE structural and functional evolution.

23

24 #Address correspondence to: David Rekosh, dr4u@virginia.edu, or Stuart Le Grice,
25 legrices@mail.nih.gov.

26

27 *C.S. and P.E.H.J. contributed equally to this work.

28

29 Abstract word count: 331

30 Text word count: 9173

31

32 **ABSTRACT**

33 **Abstract.**

34 The HIV-1 Rev Response Element (RRE) is a *cis*-acting RNA element characterized by
35 multiple stem-loops. Binding and multimerization of the HIV Rev protein on the RRE
36 promotes nucleocytoplasmic export of incompletely spliced mRNAs, an essential step in
37 HIV replication. Most of our understanding of the Rev-RRE regulatory axis comes from
38 studies of lab-adapted HIV clones. However, in human infection, HIV evolves rapidly
39 and mechanistic studies of naturally occurring Rev and RRE sequences are essential to
40 understanding this system. We previously described the functional activity of two RREs
41 found in circulating viruses in a patient followed during the course of HIV infection. The
42 “early” RRE was less functionally active than the “late” RRE despite differing in
43 sequence by only four nucleotides. In this study, we describe the sequence, function,
44 and structural evolution of circulating RREs in this patient using plasma samples
45 collected over six years of untreated infection. RRE sequence diversity varied over the
46 course of infection with evidence of selection pressure that led to sequence

47 convergence as disease progressed. An increase in RRE functional activity was
48 observed over time, and a key mutation was identified that correlates with a major
49 conformational change in the RRE and increased functional activity. Additional
50 mutations were found that may have contributed to increased activity as a result of
51 greater Shannon entropy in RRE stem-loop II, which is key to primary Rev binding.

52

53 **Importance.**

54 HIV-1 replication requires interaction of the viral Rev protein with a *cis*-acting regulatory
55 RNA, the Rev Response Element (RRE), whose sequence changes over time during
56 infection within a single host. In this study, we show that the RRE is subject to selection
57 pressure and that RREs from later time points in infection tend to have higher functional
58 activity. Differences in RRE functional activity are attributable to specific changes in
59 RNA structure. Our results suggest that RRE evolution during infection may be
60 important for HIV pathogenesis and that efforts to develop therapies acting on this viral
61 pathway should take this into account.

62

63 **INTRODUCTION**

64 All retroviruses produce mRNAs that retain introns, and these mRNAs must be
65 exported to the cytoplasm for packaging into viral particles and translation of essential
66 viral proteins. Eukaryotic cells have RNA surveillance mechanisms that would normally
67 restrict nucleocytoplasmic export and translation of these mRNA species (1). Thus,
68 retroviruses have evolved specific mechanisms to overcome this restriction (2). In HIV,

69 the Rev protein, in conjunction with its RNA binding partner, the Rev Response Element
70 (RRE), mediates this important function (3-6).

71 HIV Rev contains several well-characterized functional domains that facilitate
72 shuttling between the nucleus/nucleolus and the cytoplasm by accessing cellular
73 pathways for nuclear import and export. One of these domains is a basic, arginine-rich
74 motif that functions as a nuclear/nucleolar localization signal (7-10). This domain also
75 serves as an RNA-binding domain that binds specifically to the RRE (11, 12). It is
76 flanked on both sides by oligomerization domains that are required for Rev
77 multimerization on the RRE (13, 14). Towards the carboxy terminus is a leucine-rich
78 domain which docks on the Crm1-RanGTP complex (15) and functions as the nuclear
79 export signal (NES) (12, 16, 17).

80 The RRE is a *cis*-acting RNA element located in a highly conserved and
81 functionally important region of *env* at the N-terminus of the gp41 fusion protein (3-6). At
82 this position, it is present in all HIV RNAs that retain introns. The minimal functional
83 RRE, or “short” RRE, has been mapped in infectious laboratory clones to a 234-nt
84 region (see Figure 3). It forms a highly branched structure where the 5’ and 3’ ends pair
85 to form stem-loop I (SL-I) (18). SL-I opens into a central loop, from which several
86 additional stem loops branch out. Stem loop II contains stem IIA that branches out of
87 the central loop and opens into a three-way junction. The junction opens into stem-loops
88 IIB and IIC (19, 20). SL-III is a small stem-loop that comes off of the central loop, while
89 SL-IV and SL-V can adopt alternative topologies (21). Maximal functional activity of the
90 RRE requires a somewhat larger structure, often referred to as the “long” (351-nt) RRE,
91 characterized by an extended SL-I (18, 22, 23).

92 Primary RRE binding initiates cooperative assembly of additional Rev molecules
93 (about 6-8) in a process that requires electrostatic Rev-RRE interactions and
94 hydrophobic Rev-Rev interactions (13, 18, 24-32). Rev oligomerization on the RRE
95 increases its binding affinity ~500 fold (30). Oligomerization also arranges the NES
96 domains for binding to the RAN-GTP bound Crm1 dimer (15) forming an export-
97 competent ribonucleoprotein complex (33, 34). The complex is targeted to the nuclear
98 pore, where it interacts with the nucleoporins, resulting in its translocation to the
99 cytoplasmic side. Once in the cytoplasm, RRE-containing mRNAs are translated into
100 Gag, Gag-Pol, Env, and accessory viral proteins.

101 Molecular details of the Rev-RRE pathway have been delineated mostly from
102 studies of lab-adapted HIV clones. However, there is mounting evidence that subtle
103 variation in Rev and RRE sequences among primary isolates may contribute to
104 pathogenesis. Differences in Rev-RRE functional activity up to 24-fold were observed
105 for naturally occurring viruses in different patients (35). In addition, a study performed
106 with a Thai cohort demonstrated RRE changes over the course of infection, and higher
107 RRE activity was associated with a more rapid CD4 count decline (36). Low Rev activity
108 has also been associated with slower disease progression (37, 38) and reduced
109 susceptibility of infected cells to T-cell killing (39). In equine infectious anemia virus, a
110 related lentivirus that also utilizes the Rev/RRE axis, functional evolution of Rev has
111 been observed during infection, and Rev activity has been found to correlate with
112 disease state in ponies (40-42). Further studies of the structural and functional evolution
113 of the Rev-RRE system in natural infection are necessary to understand the role that

114 this regulatory axis plays in adaptation of HIV to diverse immune environments, and this
115 may benefit development of Rev-RRE targeted therapeutics.

116 We previously investigated the activity of Rev-RRE cognate pairs from HIV
117 isolated from five different patients at two time-points during their course of infection
118 (43). The sequences were obtained by single genome sequencing of viruses from blood
119 plasma samples and their functional activity was determined using a sub-genomic
120 reporter assay. We observed significant activity differences between Rev-RRE cognate
121 pairs from different patients and from different time points in the same patient. Evolution
122 of Rev and the RRE observed in patient SC3 was particularly striking. In this patient, the
123 RRE converged on one predominant sequence at the later time point (the M57A RRE,
124 designated here as V20-1), suggesting it was subject to strong selective pressures.
125 Furthermore, this RRE had only four nucleotide changes (mut 1-4) relative to the early
126 time point RRE (M0-A RRE, designated here as V10-2) but was 2-3 fold more
127 functionally active. Gel mobility shift assays revealed that the V20-1 RRE promoted Rev
128 multimerization at a lower concentration of Rev protein compared to the V10-2 RRE. It
129 was also notable that the predominant Rev sequence present at the early time point
130 persisted at the late time point, suggesting that the limited nucleotide changes in the
131 RRE were the major driver of differential Rev-RRE activity.

132 In the current study, we conducted a detailed examination of RRE evolution in
133 the blood plasma of patient SC3 using samples collected at six-month intervals, from
134 the time viral RNA was first detected through year six of infection. DNA deep
135 sequencing, selective 2' hydroxyl acylation analyzed by primer extension (SHAPE)
136 chemical probing, and a Rev-RRE functional assay were used to determine sequence

137 evolution, RRE secondary structure, and Rev-RRE functional activity over time and to
138 explore the mechanism underlying the observed activity differences. This study
139 highlights, for the first time, the structure-function relationship of longitudinal RRE
140 sequence evolution in a single patient and the underlying molecular mechanisms.

141

142 **RESULTS:**

143 **RRE sequence evolution in an HIV-infected individual followed over many years.**

144 Plasma samples from patient SC3 were collected over a period of 10 years
145 during standardized visits spaced about 6 months apart as part of the Women's
146 Interagency HIV Study (WIHS) Consortium in the Bronx, New York. Patient SC3 was
147 enrolled in the WIHS cohort prior to HIV seroconversion, was followed through visit 20,
148 and never received antiretroviral therapy (ART). Samples for this patient were available
149 for all time points with the exception of four missed visits (2, 3, 17 and 18). Plasma
150 samples from each WIHS visit were tested for p24 antibody and CD4 count (Figure 1).
151 Viral load was measured once the patient tested positive for p24 antibodies. In this
152 report, each visit is denominated as VXX with the numeral representing the visit
153 number. Although p24 antibodies were not detected under the original WIHS protocol
154 until V10, a significant fall in her CD4 count was noted at V08 and we were able to
155 readily amplify HIV from plasma taken at this time point, suggesting infection between
156 V07 and V08. After a short-lived rebound at V09, the CD4 count continued to fall and
157 reached a nadir of 73 cells/ μ l at V20. Seroconversion and viremia were noted in the
158 data obtained from the WIHS protocol at V10, and the viral load continued to rise
159 through V20 reaching a peak of 1.4×10^6 copies/ml. As expected without ART treatment,

160 we observed a general increase in viral load concomitant with a decline in CD4 count as
161 disease progressed.

162 We investigated RRE sequence evolution in viruses isolated from V08 and
163 onwards. A total of 12 plasma samples representing visits 7, 8, 9, 10, 11, 12, 13, 14, 15,
164 16, 19 and 20 were received from the WIHS consortium. Viral RNA isolation was
165 attempted from each sample and, if successful, RRE sequences were determined by
166 next-generation sequencing. As stated above, the first visit to yield HIV sequences that
167 could be amplified by PCR was V08. The prevalence of each RRE sequence at a given
168 visit was calculated as a percentage of the total number of sequences present at that
169 time point (Figure S1). Sequences present with a frequency of <5% were then excluded
170 from consideration, as it was not possible to distinguish true rare RREs from artifacts
171 due to PCR errors, and the prevalence of significant variants was recalculated after
172 exclusion of these minority sequences (Figures 2, S2). RRE sequences were assigned
173 a code in the form VXX-Y where XX refers to the visit number and Y refers to the
174 prevalence rank order of that sequence.

175 As shown in Figure 1, data obtained from the WIHS indicated that patient SC3
176 seroconverted to HIV-positive status at V10. Thus, in our previous study, V10 was
177 believed to represent a timepoint within six months of infection and was designated month
178 0 (M0). An RRE was identified at this visit by single genome sequencing that was
179 believed to be the major species present at that time and designated an “early” RRE.
180 Our deep DNA sequencing results showed that this “early” RRE sequence represented
181 17% of the sequences present at that visit and it is therefore labeled as V10-2 in the
182 present study. This sequence is very similar to the single founder RRE sequence found

183 at V08 (V08-1), differing only by a single nucleotide near the 3' end and mapping to the
184 right-hand side of SL-1 (designated here as mut 5). Our previous study also identified a
185 single RRE from V20 which we designated a “late” RRE. This RRE is identical with the
186 V20-1 sequence generated by deep sequencing.

187 Since the V10-2 RRE previously described as the “early” RRE has been studied
188 intensively by us, we decided to compare its properties to the founder V08-1 RRE. Both
189 RREs were transcribed *in vitro* and their secondary structures chemically probed by
190 1M7 (1-methyl-7-nitroisatoic anhydride) using selective 2' hydroxyl acylation analyzed by
191 primer extension and mutational profiling (SHAPE-MaP) (44-50). In this procedure,
192 RNAs are first modified with chemical reagents that selectively acylate unpaired
193 ribonucleotides at their 2'-hydroxyl positions, then reverse transcribed under conditions
194 that introduce mutations in cDNA opposite the sites of modification (47, 49). The
195 position and frequencies of these mutations are used to create reactivity profiles
196 indicating which RNA nucleotides are likely to be single- or double-stranded (data
197 available upon request). This information is in turn used to guide the RNAstructure
198 software (51) to generate lowest Gibbs free energy secondary structure models.

199 SHAPE-MaP studies revealed that V08-1 and V10-2 form similar structures with
200 only minor local differences (Figure 3A and 3B). These structures are similar to the
201 previously reported ARv2/SF2 RRE structure (22) where a part of the central loop (nt
202 125-130) between SL-III and SL-IV paired with nucleotides from the upper stem of SL-I
203 (193-198) forming a stem that bridges the central loop and SL-IV and SL-V.

204 To determine activity of each of these RREs, as well as V20-1, each RNA was
205 cloned into a two-color fluorescent-based proviral reporter vector (52) which carried

206 inactivating mutations in *rev*. RRE activity was measured by co-transfecting a separate
207 plasmid that expressed the previously described M0-B/M57A-SC3 Rev into 293T/17
208 cells. This Rev protein has been shown by single genome sequencing to pair with the
209 V10-2 RRE (43). It was also the unique founder Rev sequence present at V08.
210 Unexpectedly, this sequence still persisted at V20 and was found in single genomes
211 with the V20-1 RRE (43). The reporter construct expressed eGFP from the intron-
212 containing Rev-dependent *gag* mRNA and TagBFP from the intron-less Rev-
213 independent *nef*-like transcript. Thus, in this assay, the ratio of the fluorescent signals
214 (eGFP:TagBFP) is a measure of Rev-RRE functional activity. Control experiments
215 showed that the assay is highly sensitive to the addition of Rev. For example, when
216 increasing the amount of Rev plasmid in the assay system from 0 ng to 100 ng, there is
217 a 268-fold increase in GFP expression with only a slight decrease in BFP expression
218 (2.6 fold) (52).

219 All three RREs displayed clear Rev responsiveness as the fluorescent ratio in the
220 non-Rev containing transfections was at least 500-fold less than in Rev-containing
221 transfections (data not shown). Despite their local structural differences, both V08-1 and
222 V10-2 RRE showed similar levels of RRE activity ($p=0.999$) (Figure 4). Therefore,
223 although mutation 5 arose after infection and increased in prevalence through V20, it
224 did not increase RRE functional activity or significantly change RRE structure.
225 Additionally, activities of V08-1 and V10-2 RREs were substantially less than that of
226 V20-1 (Figure 4) ($p=0.022$ and $p=0.021$, respectively), consistent with our previous
227 finding that V20-1 RRE is more active (43). Notably, we also replicated the finding that
228 V20-1 is significantly more active than V10-2 using a lentiviral vector system, where

229 packaging of genomic RNA and titer is dependent on Rev-RRE function (data available
230 upon request) (35, 53) .

231

232 **V10-2 and V20-1 RREs form distinctly different secondary structures.**

233 We previously reported that there are only four single nucleotide changes (mut 1-
234 4) between the V10-2 and V20-1 RREs (43). A fifth mutation (mut 5) is present in both
235 V10-2 and V20-1 and therefore did not score as a difference between the two RREs
236 identified as “early” and “late” in our previous study. On a canonical 234-nt five stem-
237 loop (5SL) RRE structure (21), these changes map near the apical loop of SL-IIB [nt 61:
238 mutation (mut) 1] and SL-IIC [nt 84: mutation (mut) 2], the central loop region between
239 SL-V and SL-I [nt 194: mutation (mut) 3], and at the base of stem of SL-I [nt 228:
240 mutation (mut) 4] (see Figures 3B and 3D). We next explored whether the differences in
241 activity between the two RREs could be attributed to structural differences caused by
242 any individual nucleotide change.

243 *In vitro* transcribed and folded V10-2 and V20-1 short RREs migrated at a
244 significantly different rate when analyzed by native polyacrylamide gel electrophoresis
245 (Figure 3E), suggesting major structural differences. Consistent with the gel migration
246 data, SHAPE-MaP of the two 234-nt RREs revealed that the V10-2 and V20-1 RREs
247 adopt distinctly different conformations (Figures 3B and 3D). Unlike V10-2, which had
248 part of the central loop region base-paired, V20-1 formed the canonical 5SL structure
249 where five distinct stem-loop structures (SL-I to SL-V) radiate out directly from the single
250 stranded central loop.

251 Closer analysis of the location of each of the four nucleotide changes suggested
252 that the major structural shift in the two RREs might have been caused by mut 3. The
253 nucleotide at the mut 3 position (G) is base-paired in the bridging stem in V10-2. In V20-
254 1, it mutates to C disrupting base pairing at this position thereby destabilizing the stem
255 formed by nt 125-130 and 193-198. Consequently, nt 34-36 were significantly more
256 reactive while nt 125, 127, and 130 were significantly less reactive in V10-2 compared
257 to V20-1. Mut 1 and mut 2 produced more limited local structural changes, i.e. opening
258 and formation of the base-pair near the apical loop of SL-IIB and SL-IIC in V20-1
259 relative to V10-2. Since mut 4 was located at the primer-hybridization site (see the
260 PCR1 step of SHAPE-MaP in Methods) for the 234-nt RREs, we were unable to assess
261 its effect on the secondary structure.

262 A 3-dimensional structural analysis of a 351-nt RRE by small angle X-ray
263 scattering has shown that the extended SL-I folds back on regions in and around SL-II
264 to expose a cryptic Rev-binding site (22). Data obtained in connection with our previous
265 study (43), showed that the extended SL-I of the 351-nt V10-2 and V20-1 RREs has an
266 additional four nucleotide changes at nucleotide positions 13, 27, 29, and 57 (using the
267 351-nt RRE numbering system). We therefore investigated if these nucleotide changes
268 in the extended SL-I affect RRE structure. Additionally, probing these extended RREs
269 provided an opportunity to determine the effect of mut 4 on their structure, as this
270 position no longer fell on the primer hybridization site during SHAPE analysis of the
271 351-nt RREs. The long RREs were investigated by capillary electrophoresis-based
272 SHAPE (Figure 5) (CE-SHAPE) using N-methylisatoic anhydride (NMIA) as the
273 electrophile (54, 55). CE-SHAPE differs from SHAPE-MaP in that the chemically

274 modified nucleotides are identified as stops during primer extension. CE-SHAPE
275 analysis of the 351-nt V10-2 and V20-1 revealed that mut 4 did not produce any
276 structural changes between V10-2 and V20-1 RREs, as it changed a U-A base pair to
277 U-G. Additionally, the nucleotide differences in the extended SL-I region of these RREs
278 produced only highly localized structural changes, if any. Changes at nt 13 and nt 57
279 produced no structural changes at all, whereas nucleotide differences at nt 27 and nt 29
280 induced opening of base pairs at these positions in V20-1. As these mutations in SL-1
281 did not alter the structure of the comparable region of the 234-nt RRE, subsequent
282 studies investigated their effects only in the short RRE forms.

283

284 **Structural and functional analysis of patient SC3 RREs containing individual** 285 **single nucleotide mutations.**

286 We next investigated the contribution of each of the four nucleotides which
287 differed between the V10-2 and the V20-1 RREs to alterations in structure and
288 functional activity. To this end, we created four new synthetic 234-nt RRE sequences,
289 each containing one of the single nucleotide changes in a V10-2 RRE background. The
290 new RREs containing mut 1, 2, 3, and 4 were respectively termed M1, M2, M3, and M4.
291 The secondary structure of each RRE was probed by SHAPE-MaP (Figure 6A-D). As
292 predicted, M1, M2, and M4 RREs formed V10-2 like structures, whereas M3 RRE
293 formed a V20-1 like structure. M1 RRE resembled V10-2 RRE with the exception that
294 the G to A mutation eliminated a base pair adjacent to the SL-II apical loop. Similarly,
295 M2 RRE differed from V10-2 RRE only in the formation of an extra base pair next to the
296 apical loop of SL-IIC. M4 RRE formed a structure identical to V10-2 RRE, since the mut

297 4 A to G change preserved non-canonical base pairing at this position by replacing A-U
298 with a G-U base pair. The major structural shift involving the central loop, SL-IV, SL-V,
299 and SL-I between the V10-2 and V20-1 RREs was reproduced by the single G to C
300 mutation in the M3 RRE. Therefore, we reasoned that mut 3 might be the major driver of
301 the functional difference between the V10-2 and V20-1 RREs.

302 We next measured the contribution of each mutation to the functional activity
303 difference between the V10-2 and V20-1 RREs in 293T/17 cells (Figure 6E). Activity of
304 RREs M1-M4 was determined using the fluorescent-based transient proviral reporter
305 with the same cognate SC3 Rev used in Figure 4. As before, in the presence of SC3
306 Rev, functional activity of V20-1 RRE was significantly higher than that of V10-2 RRE
307 ($p=0.001$). Among all single SC3 mutants, only M3 displayed activity that was
308 statistically significantly higher than V10-2 ($p=0.072$) even though it did not quite reach
309 the activity level of V20-1. M1 and M2 RREs were only slightly more active than V10-2
310 but these differences did not reach statistical significance. Activity of M4 RRE was also
311 not statistically distinguishable from that of V10-2. However, M4 had a tendency
312 towards lower, rather than higher, functional activity. Thus, the difference in functional
313 activity between V10-2 and V20-1 could not be explained by any single nucleotide
314 mutation.

315

316 **Structural and functional analysis of selected RRE sequences derived from** 317 **patient SC3 at different time points.**

318 To further understand how specific sequence changes between V10-2 and V20-1
319 RREs affected functional activity, we studied intermediate RRE sequences from viruses

320 that arose during disease progression in patient SC3. SC3 RREs that allowed us to test
321 combinations of these mutations in the order they appeared in the natural isolates were
322 selected from this evolutionary data set (Figure 2; Figure S2). The secondary structure
323 and functional activity of these RREs were then determined by SHAPE-MaP and the
324 fluorescent-based reporter assay, respectively.

325 The position designated mut 3 starts as a G in V08-1, remains a G in V10-2,
326 changes to A in many sequences in V09 through V16, and then to C in V19 and V20. As
327 this is the position that causes the major structural shift between V10-2 and V20-1, we
328 sought to determine if the A at the mut 3 position would result in the same structure as
329 its replacement by C. To test this, we determined the secondary structure of V09-2 RRE
330 by SHAPE-MaP and compared it to the structure of V08-1 and V10-2 (Figure 3A-C).
331 The V09-2 RRE sequence is identical to V08-1 except at the mut 3 position, where the
332 G in V08-1 is replaced with A. We hypothesized that if disruption of the G-C base-pair at
333 this position induced the structural shift observed between V10-2 and V20-1, then such
334 a shift should also be reflected between V08-1 and V09-2. Indeed, the secondary
335 structure of V09-2 resembled that of V20-1 RRE, confirming our hypothesis. V09-2 RRE
336 was also slightly more active than V08-1 RRE (though this trend did not reach statistical
337 significance) ($p=0.116$) and V10-2 ($p=0.027$) (Figure 7). Consistent with our previous
338 observation with M3 RRE, the structural shift invoked in V20-1 and V09-2 relative to
339 V08-1 and V10-2 shows a trend towards increased SC3 RRE activity.

340 Mut 2 was first noted in the sample from V11 and was present in all RRE
341 sequences from subsequent visits. We tested the V11-1 RRE as it provided the
342 opportunity of investigating the combination of mut 2 together with A in the position of

343 mut 3. Although it was predicted to have higher activity than M3 and V09-2 RRE, V11-1
344 RRE had similar level of RRE activity as the founder RRE, V08-1, suggesting that while
345 A at the position of mut 3 increases functional activity alone, it does not do so in the
346 context of the additional mut 2 ($p=1.000$).

347 We first detected mut 1 in plasma samples from visit 13. This mutation was
348 frequently observed on subsequent visits and was present in the majority of RREs from
349 visit 15 onwards. The V13-1 RRE contained not only mut 1 but also mut 2 and A in the
350 mut 3 position. This RRE had significantly higher activity than both the V08-1 and V09-2
351 variants ($p<0.001$ for both comparisons). Therefore, mut 1 not only contributes to RRE
352 activity in itself but also rescues the activity of the combination of mut 2 and an A in the
353 mut 3 position.

354 We also tested the activity of V14-2, which allowed us to test the combined
355 phenotype of mut 1, mut 2, A in the mut 3 position, and mut 5. Activity of this RRE did
356 not significantly differ from V13-1, suggesting that acquisition of mut 5 does not
357 contribute to RRE activity ($p=0.332$). However, activity of the V20-1 RRE, which harbors
358 C in the position of mut 3 rather than the A of V13-1, as well the other mutations, was
359 significantly higher than V13-1 ($p<0.001$). This suggests that C in the mut 3 position is
360 important for imparting higher RRE activity when all other mutations are present. It is
361 also possible that although mut 4 does not contribute to RRE activity individually, it can
362 contribute to activity when combined with the other additional changes.

363 This set of SC3 RREs permitted examination of changes in functional activity
364 over time. Activities of V08-1, V10-2, and V11-1 were very similar, demonstrating that
365 the combinations of mutations observed in these sequences are not sufficient in

366 themselves to confer higher functional activity. V13-1 was the first tested RRE to arise,
367 other than V09-2, that showed significantly higher activity than V08-1 and it did so with
368 the combination of mut 1, mut 2, and A in the mut 3 position. The accumulation of
369 additional changes in V14-2 (addition of mut 5), V19-2 (addition of mut 4, the A to C
370 change at mut 3, and an additional A to G change at nt 142), and V20-1 (reversion of nt
371 142 to A) corresponded to a trend towards increasing functional activity at each step.
372 This steady trend suggests functional evolution of the RRE in the later phase of the
373 disease course of patient SC3, as new combinations of mutations arose and those
374 conferring greater functional activity showed preferential selection.

375

376 **Shannon entropy profile of SC3 RRE variants and single mutants.**

377 Since the energetically most favorable secondary structures of SC3 RRE variants
378 and single mutants were insufficient to explain the functional activity differences
379 observed between the V08-1 and V20-1 RREs, we next assessed the ability of the RREs
380 to adopt alternative conformers by evaluating their SHAPE-guided Shannon entropies
381 and base pairing probability at single nucleotide resolution. Shannon entropies were
382 calculated based on the probability for each base-pair appearing across all possible
383 structures predicted for the RNA. Regions with highly stable well-defined RNA
384 structures are characterized by lower Shannon entropies. Conversely, regions with high
385 Shannon entropy are likely to form alternative conformers.

386 We compared Shannon entropy profiles of the V08-1, V09-2, V10-2, V20-1, M1,
387 M2, M3, and M4 SC3 RREs (Figure 8). Most regions of these RREs exhibited low
388 Shannon entropy, suggesting their overall secondary structures are highly stable. This

389 result is consistent with the observation that these RRE RNAs migrate as a single
390 discrete band on a native agarose gel, suggesting a high degree of structural
391 homogeneity (data available upon request).

392 However, we observed differences in Shannon entropy values at two different
393 regions. Specifically, values of the loop regions between SL-IIA and SL-IIB (Region I)
394 and between SL-IIB and SL-IIC (Region II) varied between RREs. The values for the
395 V20-1 RRE were, respectively, 5-6 fold and 4 fold higher than for the V08-1 and V10-2
396 RREs, suggesting that the nucleotides in these two regions of the V20-1 RRE are not
397 always single-stranded as depicted in the secondary structures generated by SHAPE-
398 MaP. This finding is further corroborated by SHAPE-MaP-guided base pairing
399 probability calculated for each of these RREs (data available upon request), which
400 shows that the two higher entropy regions of V20-1 RRE can base-pair with each other
401 with a probability of 10-80%. Both the Shannon entropy and pairing probability data
402 suggest that these two regions of V20-1 RRE are structurally dynamic, a feature that
403 confers accessibility to protein interaction with the RNA by serving as landing pads for
404 protein cofactors (44). This accessibility may have implications for Rev-binding, possibly
405 contributing to the higher activity of V20-1 RRE.

406 Furthermore, both the V09-2 and M3 RREs have 2-fold higher Shannon entropy
407 for the loop region between SL-IIA and SL-IIB (Region I) compared to V08-1 and V10-2
408 RREs. Their entropy values for the nucleotides between SL-IIB and SL-IIC (Region II),
409 however, did not change relative to V08-1 and V10-2. While both V09-2 and M3
410 undergo the structural shift characteristic of V20-1 and are modestly more active than
411 V08-1 and V10-2, the inability of V09-1 and M3 RREs to reach the degree of structural

412 flexibility of the V20-1 RRE in the internal loop of SL-II might explain why these RREs
413 are not as functionally active as V20-1. The Shannon entropy profile of M2 RRE is
414 similar to the M3 and V09-1 RREs, whereas M1 RRE has 2-fold higher Shannon
415 entropy than V08-1 and V10-2 in both regions of SL-II. The modestly higher entropy in
416 the M1, M2, and M3 RREs relative to V08-1 and V10-2 might help to explain their trend
417 towards higher functional activity (Figure 6). The M4 RRE, on the other hand, did not
418 show any increase in entropy over V08-1 and V10-2 and also displayed similar or lower
419 functional activity.

420 Taken together, our analysis suggests that both the major structural shift
421 observed between the V08-1 and V20-1 RREs, and possibly also that the difference in
422 structural dynamism in the internal loop of SL-II contribute to the significant increase in
423 functional activity over time.

424

425 **DISCUSSION**

426 In this study, we describe a complex relationship between RRE structure and
427 functional activity using naturally occurring sequences obtained from a single patient.
428 This study is the first detailed examination of longitudinal evolution of the HIV-1 RRE
429 over about six years of naturally occurring infection and demonstrates clear selection
430 pressures acting on the RRE sequence with a tendency towards increased functional
431 activity over time. Increased activity can be explained by large-scale conformational
432 changes within the RRE and a decrease in base-pairing stability at the initial Rev-
433 binding site in SL-II.

434 The evolution of the RRE sequence is strongly suggestive of selection pressures
435 operating on the RRE itself. The single founder RRE sequence found at visit 8
436 diversifies initially, and by visit 20 converges on only a single circulating RRE sequence
437 differing from V08-1 by five single nucleotides. The early appearance and persistence of
438 mutations at only a few locations, as well as the reduced viral diversity by visit 20, argue
439 that the phenotype resulting from these changes was subject to strong selection
440 pressures. Functional activity analysis of the SC3 RREs suggests that the RREs with
441 higher activity were selected as disease progressed, with the early time-point RREs
442 (V08-1 and V10-2) displaying the lowest and the late time-point RRE (V20-1) displaying
443 the highest functional activity. The tendency towards increased functional activity
444 corresponded with gradual accumulation, in different combinations, of five mutations
445 that characterize V20-1 relative to V08-1.

446 There is no direct correspondence between specific mutations and functional
447 activity phenotypes. Changes at the mutation 3 position predicted to disrupt base-
448 pairing appear to result in an activity increase. However, V09-2 RRE containing this
449 change alone still has significantly lower activity than V20-1, showing that the other
450 mutations also contribute to a change in RRE activity in combination. While all
451 mutations 1-5 are necessary to achieve the highest activity, their contributions are not
452 merely additive. For example, V11-1 resembles V09-2 with the addition of mut 2, but it
453 does not have increased activity relative to the founder. Additionally, mutations which
454 have no impact on activity in isolation can increase activity in combination. For example,
455 mut 4 does not change activity alone, but is responsible for the increase in activity
456 between V14-2 and V20-1 in the context of the other four mutations.

457 Two types of structural changes were uncovered in this study that can explain
458 differences in activity: major conformational changes and regions of increased base-
459 pairing entropy. Previously, we have shown that alternative conformations of the
460 laboratory strain NL4-3 RRE display significantly different activities, with a four stem-
461 loop conformation supporting lower replicative capacity than a five stem-loop structure
462 (21). In this study, we found that the higher activity RRE (V20-1) forms a five stem-loop
463 conformation resembling that observed for NL4-3, while the lower activity RREs (V08-1
464 and V10-2) adopt a different conformation with a more collapsed central loop. As
465 expected from functional analysis of the M3 and V09-2 RREs, both the G to A (V09-2)
466 and G to C (M3) changes at the mutation 3 position induce a five stem-loop structure
467 associated with increased activity. The additional mutations were not individually
468 associated with large-scale conformational changes in SHAPE-MaP modeling.

469 The combination of mutations 1-5, though not each mutation in isolation, also
470 corresponds to increased Shannon entropy in stem-loop II. This is the region where the
471 first and second dimers of Rev bind (56). The disordered base pairing in this region,
472 implied by greater entropy, may facilitate Rev-RNA binding at the primary Rev binding
473 site and subsequent multimerization leading to enhanced activity. This is consistent with
474 our previous *in vitro* gel-shift observations (43) that demonstrated the ability of the V20-
475 1 RRE to promote Rev multimerization more efficiently than the V10-2 RRE. In the
476 absence of major conformational changes attributable to mutations 1, 2, 4, and 5, this
477 mechanism may account for the difference in functional activity between the RREs
478 containing unpaired nucleotides at mutation 3 position (e.g. V09-2 and M3) that lack

479 these additional mutations and the V20-1 RRE. It remains unclear how the presence of
480 these mutations in combination results in increased stem-loop II entropy.

481 This study also provides further support for the hypothesis that the Rev-RRE
482 regulatory axis plays an important role in HIV pathogenesis. An important consideration
483 in the interpretation of these findings is that all five mutations in V20-1 relative to V08-1
484 are nonsynonymous in the overlapping gp41 coding sequence, raising the possibility
485 that changes in Env could contribute to the selective pressure. We searched for known
486 CTL epitopes in the Env ORF overlapping the V08-1 RRE sequence using the Los
487 Alamos HIV database Epitope Location Finder tool (www.hiv.lanl.gov). CTL epitopes
488 have been described in the V08-1 regions containing three of the five mutations
489 (mutations 3, 4, and 5). Thus, selection of these mutations could plausibly reflect
490 immune evasion, though it is notable that neither mutation 3 nor 5 were consistently
491 found in all RRE sequences at all time points after they were first observed at visits 9
492 and 10.

493 While the selection evidenced by sequence convergence at visit 20 might be due
494 to pressure on Env in terms of immune evasion, replication efficiency, or other factors, it
495 is likely that functional differences in Rev-RRE activity also play a significant role in
496 overall viral fitness. Nucleotide changes at the mutation 3 position highlight this
497 likelihood. The nonsynonymous mutations from G to A at visit 9 and A to C at visit 19
498 are both consistent with CTL evasion. From the standpoint of the RRE, however, the G
499 to A change shifts the RRE structure to a higher activity conformation while A to C is
500 structurally and functionally neutral. Thus, the A to C mutation preserves high RRE
501 activity while also modifying the Env amino acid sequence. Convergence of circulating

502 RRE sequences by visit 20 is particularly striking in light of the very low CD4 count at
503 this time point, as viral fitness would likely have been more influenced by Rev-RRE
504 activity than by immune surveillance.

505 We were unable to assess functional evolution of the Rev protein over time in
506 this study due to the sequencing strategy used, which created reads too short to allow
507 linkage of both of the Rev coding exons and the RRE. However, previous work using
508 single genome sequencing with samples from this patient (43) demonstrated that a
509 single Rev amino acid sequence was most prevalent at both visits V10 and V20. This is
510 the Rev sequence that was used in this study. Its persistence throughout the entire
511 infection period suggests that it likely occurred in conjunction with most or all of the
512 RREs tested here. It is also notable that m6A methylation of RRE RNA has recently
513 been proposed as an additional mechanism of modulating HIV replication capacity (57).
514 This was not assessed in the present study but could additionally contribute to
515 differences in Rev-RRE activity.

516 The generalizability of the findings described here awaits further longitudinal
517 studies, analyzing both Rev and RRE sequences, in patients with varying courses of
518 disease. A clear understanding of RRE evolution during natural infection will help to
519 further our understanding of the role that this regulatory axis may play in key aspects of
520 the viral life cycle, including transmission and the establishment of latency. Furthermore,
521 since the Rev-RRE interaction is an essential step in viral replication, it is also a
522 promising target for drug development. This study demonstrates that RRE structures
523 can vary over the course of natural infection, and thus that rational drug design must
524 account for the spectrum of potential Rev-RRE interaction conformations.

525

526 **MATERIALS AND METHODS**

527 **Clinical samples and ethics statement.**

528 All studies involving human subjects were approved by the institutional review
529 board at Montefiore Hospital, Bronx, NY, as part of the Women's Interagency HIV Study
530 (WIHS). Written informed consent was provided by all study subjects. Plasma samples
531 from one patient (SC3), collected over a period of seven years, were obtained from the
532 WIHS Consortium, Bronx, NY (Kathryn Anastos, principal investigator), as previously
533 described (43). A total of 11 samples representing different time points were received
534 for analysis.

535

536 **Viral RNA extraction and cDNA synthesis.**

537 Viral RNA was extracted from 1 ml of plasma using a guanidinium extraction
538 protocol (58). Viral cDNA synthesis was performed immediately after viral RNA was
539 extracted as described (43). Briefly, each viral RNA pellet was resuspended in 40 μ l of 5
540 mM Tris-HCL, pH 8.0, prior to cDNA synthesis with 50 μ M of oligo(dT) and 100 U of
541 Superscript III per reaction (Invitrogen, Carlsbad, CA). The reverse transcription
542 reaction was incubated at 50°C for 1 hour, then 55°C for 1 hour and then 70°C for 15
543 minutes, after which 4 units of RNase H (Invitrogen) were added, and samples
544 incubated at 37°C for 20 minutes. Samples were stored at -80°C prior to amplicon
545 generation.

546

547 **PCR amplification and purification.**

548 Amplicons (~3 kb) spanning both HIV Rev exons and the RRE, were produced
549 for each time point. The first round PCR reaction was performed by adding 1 µl of
550 cDNA template to a 20 µl reaction containing 0.005 U of Platinum Taq Hi-Fidelity
551 polymerase (Invitrogen) as previously described (59). Using 1 µl of the first round PCR
552 product as a template, nested PCR resulted in amplicons ~3 kb in length. Primers for
553 the first round PCR reaction were 2302 (5'-aagccaccttgcttagtg-3') and 2278 (5'-
554 ttgctactgtgattgctccatgt-3') while those for the nested PCR were 2277 (5'-
555 tagagccctggaagcatccaggaag-3') and 2280 (5'-gtctcgagatactgctcccacc-3') (43).
556 Amplicon size was verified by agarose gel electrophoresis.

557 Each 20 µl PCR reaction was purified with 36 µl of AMPure XP beads
558 (Agencourt). After addition of beads, samples were pipetted up and down 10 times and
559 incubated at room temperature for 10 minutes prior to being placed on a magnetic
560 stand. After a 2 minute incubation, supernatant was removed and the beads were
561 washed twice with 80% ethanol. After beads were air-dried on a magnetic stand for 10
562 minutes, they were removed from the magnet, resuspended in 52.5 µl of elution buffer,
563 and incubated at room temperature for 2 minutes. Beads were then placed on the
564 magnetic stand for 2 minutes, or until the supernatant was cleared. The cleared
565 supernatant containing the purified PCR amplicons was removed and placed in a new
566 96-well plate then stored at -20°C.

567

568 **DNA library preparation and sequencing.**

569 Prior to preparing the DNA library, purified amplicon products were quantified
570 with the dsDNA HS (high sensitivity) assay kit (Invitrogen) using the Qubit 2.0

571 fluorometer (Invitrogen). The DNA library was prepared using the standard Nextera XT
572 DNA library preparation protocol (Illumina). A total of 1 ng of input DNA for each sample
573 was added to the reaction buffer which fragments the input DNA and adds adapter
574 sequences to the ends to allow for PCR reactions downstream in the library preparation
575 process. A brief PCR cycle followed the fragmentation protocol to add indexes used to
576 identify each individual sample and additional sequences for proper cluster formation.
577 PCR samples were purified and size-selected for 300-500 bp amplicons using 25 μ l of
578 AMPure XP beads. Amplicons were pooled together in equimolar concentrations then
579 sequenced with the Illumina MiSeq Reagent Kit v3 (600 cycles).

580

581 **RRE sequence analysis.**

582 Paired end reads for each time point were generated using an Illumina MiSeq.
583 The two overlapping paired reads were merged using FLASH (60), a plugin in Geneious
584 (Biomatters, Auckland, New Zealand) to produce a single read for each pair. These
585 reads were then aligned to the NL4-3 genome and reads overlapping the RRE were
586 extracted. Extracted reads were filtered for individual reads that spanned the full length
587 of the short RRE. These reads were assembled into contigs using the Geneious *de*
588 *novo* assembly tool, set for a minimum overlap identity of 100% and a minimum overlap
589 of the entire 234-nt minimal RRE. The frequency of each contig was calculated based
590 on the number of reads assigned to each contig. Contigs comprising less than 5% of the
591 total reads were then removed from each time point (to eliminate minor HIV species
592 and/or potential PCR errors) and the frequencies of the remaining contigs were
593 recalculated based on the total number of reads remaining. The sequence of each

594 contig was then aligned to the sequence from the major V08 contig to generate the
595 alignment shown in Figure 2 (see also Figures S1 and S2). RREs were named using
596 the format VXX-Y where XX corresponds to the WIHS cohort visit number at which the
597 plasma sample generating the sequence was obtained and Y corresponds to the
598 frequency rank order of the sequence. Thus, V10-2 refers to the second most prevalent
599 RRE from the sequencing of the plasma sample obtained at WIHS visit 10.

600

601 ***In vitro* transcription of RRE RNAs.**

602 RRE RNAs were *in vitro* transcribed by T7 RNA polymerase using the
603 MEGAscript kit (Life Technologies) per manufacturer's guidelines. Templates for
604 *in vitro* transcription were generated by PCR amplification of RREs from plasmids
605 containing synthetic sequences (Integrated DNA technologies) using oligonucleotides
606 designed to introduce both a T7 promoter sequence at the 5' end of the 234-nt and 351-
607 nt RREs and a structure cassette at the 3' end of the 351-nt RREs (Table S1). Plasmids
608 used for generating transcription DNA template for the 234-nt V08-1, V09-2, V10-2,
609 V20-1, M1, M2, M3, and M4 RREs were designated pHR 5334, pHR 5766, pHR 4784,
610 pHR 4788, pHR 5326, pHR 5328, pHR 5330, and pHR 5332, respectively. Those used
611 to generate 351-nt V10-2 and V20-1 RREs were designated pHR 5321 and pHR 5322,
612 respectively. *In vitro* transcription reactions were treated with Turbo DNase I (Life
613 Technologies) for 1 hr at 37°C to digest the DNA template, heated to 85°C for 2 min,
614 and RNA was fractionated on a denaturing gel (5% polyacrylamide (19:1), 1x TBE, 7M
615 urea) at constant temperature (45°C, 30W max). RRE bands were located by UV

616 shadowing, excised, electroeluted at 200 V for 2 hours at 4°C, ethanol precipitated, and
617 stored at 4°C in TE buffer (10 mM Tris, pH 7.6; 0.1 mM EDTA).

618

619 **Folding and SHAPE-MaP profiling of RRE RNA.**

620 For each RNA, 1M7 (+), 1M7 (-), and denaturation control reactions were
621 generated. Approximately 5 pmoles of RRE RNA was incubated with renaturation buffer
622 (1X: 10 mM Tris, pH 8.0, 100 mM KCl, 0.1 mM EDTA) in a total volume of 5 µl, heated
623 to 85°C, and renatured by slow cooling (0.1°C/sec) to 25°C. Renatured RNA was
624 incubated with RNA folding buffer (1X: 35 mM Tris pH 8.0, 90 mM KCl, 0.15 mM EDTA,
625 5 mM MgCl₂, 2.5% glycerol) in a total volume of 9 µl at 37°C for 30 min. RNA was
626 modified by addition of 1 µL of 25 mM 1M7. The negative control reaction contained 1
627 µL of DMSO instead of 1M7. The denaturation control was produced by incubating 5
628 pmoles of RNA with denaturation buffer (1X: 50% formamide, 50 mM HEPES, and 4
629 mM EDTA) in a volume of 9 µL at 95 °C for 1 min. 1 µL of 20 mM 1M7 was added and
630 the mixture incubated at 95 °C for another 1 min. RNA from 1M7 (+), 1M7 (-), and
631 denatured control reactions were recovered by ethanol precipitation, resuspended in TE
632 buffer (10 mM Tris, pH 7.6; 0.1 mM EDTA), and stored at -20°C.

633

634 **Mutational profiling of modified RNA.**

635 RNA from 1M7 (+), 1M7 (-), and denatured control reactions were reverse
636 transcribed using corresponding oligos to generate a cDNA library (Table S1). Reverse
637 transcription was performed by first annealing 2 µM of RT oligo to the RNA in a reaction
638 volume of 11 µL by incubation at 65 °C for 5 min, followed by cooling on ice. cDNA

639 synthesis was initiated by incubating the annealing mixture with 8 μ L of 2.5X RT
640 reaction mixture (2.5X: 125 mM Tris (pH 8.0), 187.5 mM KCl, 15 mM MnCl₂, 25 mM
641 DTT and 1.25 mM dNTPs) and 1 μ L of Superscript II RT (Thermo Fisher, 200 U/ μ L) for
642 42 °C for 3 hours. The RNA template was then hydrolyzed by adding 1 μ L 2 N NaOH,
643 followed by neutralization by addition of 1 μ L 2N HCl. The cDNA library was purified
644 using G50 spin columns (GE Healthcare).

645 For mutational profiling, cDNA was converted to dsDNA with Illumina adapters
646 for high throughput sequencing on an Illumina platform. This was achieved in two
647 consecutive PCR reactions, namely PCR1 and PCR2. The first reaction (PCR1)
648 appended partial Illumina adapters to the ends of the amplicons. The entire cDNA
649 library was used as template in a 100 μ l PCR1 reaction (1.1 μ L each of 50 pmoles of
650 forward and reverse oligo, 2 μ L of 10 mM dNTPs, 20 μ L of 5x Q5 reaction buffer, 1 μ L
651 of Hot Start High-Fidelity DNA polymerase (NEB)) using cycling conditions: 98°C for 30
652 sec, 15 cycles of (98 °C for 10 sec, 50 °C for 30 sec, 72 °C for 30 sec), 72 °C for 2 min.
653 PCR product was gel purified and 10% was used as template DNA in the PCR2
654 reaction. The PCR2 completed the Illumina adapters while adding appropriate
655 barcoding indices. The PCR2 reaction and cycling conditions were as those for PCR1.
656 The resulting amplicon library was fractionated through a 2% agarose gel and
657 amplicons purified from the gel slices by electro-elution at room temperature for 2 hr
658 followed by ethanol precipitation. Each amplicon library was quantified by real time PCR
659 using the KAPA Universal Library Quantification Kit (Illumina) per manufacturer's
660 protocol. Sequencing libraries were pooled and mixed with 20% PhiX and sequenced
661 on an Illumina MiSeq to generate 2 X 150 paired-end reads. Sequence files were fed

662 into ShapeMapper (v1.2) software (49) to generate SHAPE reactivity profiles by aligning
663 the reads to 234-nt RRE RNA sequence using the software with default settings.
664 Reactivity values obtained from ShapeMapper were input to RNAstructure software (51)
665 to generate the minimum free-energy RNA secondary structure model.

666

667 **RRE gel migration assay.**

668 RRE structural homogeneity was assessed by comparing the migration rate of the
669 folded RREs on native agarose and polyacrylamide gels. Approximately 20 pmoles of
670 RNA was suspended in 5 μ l renaturation buffer (1X: 10mM Tris, pH 8.0, 100mM KCl,
671 0.1mM EDTA), heated to 85°C, and renatured by slow cooling (0.1°C/sec) to 25°C.
672 Renatured RNA was incubated with 5 μ l of 2X RNA folding buffer (1X:70 mM Tris pH
673 8.0, 180 mM KCl, 0.3 mM EDTA, 10 mM MgCl₂, 5% of glycerol) at 37°C for 30 min, and
674 fractionated through a native 8% polyacrylamide gel (29:1) run for 22 hours at 4°C or on
675 a 2% native agarose. RRE bands were visualized by UV shadowing and ethidium
676 bromide staining, respectively.

677

678 **Plasmid constructs for functional assays of Rev-RRE activity.**

679 Functional activity of Rev-RRE pairs was determined by means of a
680 fluorescence-based transient transfection assay. To test RRE sequences, a plasmid
681 containing a near full length NL4-3 HIV-1 sequence (61) was modified to express blue
682 fluorescent protein (BFP) in a Rev-independent fashion and green fluorescent protein
683 (GFP) in a Rev-dependent fashion. The native 351-nt RRE within *env* was flanked by
684 XmaI and XbaI sites to permit exchange of this sequence with other RREs of interest.

685 Additional modifications were made to ensure the construct was not replication-
686 competent and could not express Rev. To create additional RRE constructs, the native
687 RRE was removed by digesting the plasmid with XmaI and XbaI. Commercially
688 synthesized 234-nt RRE sequences of interest with appropriate flanking sequences
689 (Integrated DNA Technologies) were then cloned into the opened *env* region using
690 Gibson assembly.

691 Rev was provided *in trans* using one of two constructs. The predominant Rev
692 previously identified at V10 and V20 by single genome sequencing had identical amino
693 acid sequences. This Rev was designated M0-B/M57-A and used for functional assays
694 except as otherwise noted (43).

695 For the analysis described in Figure 4, the M0-B/M57-A *rev* sequence was
696 cloned into a CMV expression plasmid. For the remaining functional assays, a separate
697 Rev-expressing construct was created by modifying the murine stem cell virus
698 construct, pMSCV-IRES-mCherry FP (Addgene plasmid # 52114), to express both the
699 M-0B/M57-A Rev and the mCherry fluorescent protein by means of a bicistronic
700 transcript including an internal ribosome entry site (62). The MSCV vector was a gift
701 from Dario Vignali (unpublished). Constructs utilized in the functional assays are listed
702 in Table S2.

703

704 **Selection of RREs for functional analysis.**

705 Both naturally occurring RREs sequenced from patient SC3 and synthetic RREs
706 containing individual mutations of interest were tested for functional activity. All RREs
707 tested were 234-nt in length. The naturally occurring RREs assessed were V08-1, V09-

708 2, V10-2, V11-1, V13-1, V14-2, V19-2, and V20-1. Additionally, synthetic RREs were
709 created based on single nucleotide differences between the sequences of V10-2 and
710 V20-1. The mutation 1 RRE (M1) is identical to V10-2 with the exception of a G to A
711 change at position 61, reflecting the G to A change seen at that position in V20-1. The
712 mutation 2 RRE (M2) is identical to V10-2 with the exception of a T to A change at
713 position 84. Of note, this RRE sequence was also observed to occur naturally as
714 sequence V12-1. The mutation 3 RRE (M3) is identical to V10-2 with the exception of a
715 G to C change at position 194. The mutation 4 RRE (M4) is identical to V10-2 with the
716 exception of an A to G change at position 228.

717

718 **Rev-RRE functional activity assays.**

719 RRE-containing constructs were designed such that GFP expression occurs in a
720 Rev-dependent fashion while BFP expression occurs in a Rev-independent fashion. In
721 cells transfected with both the RRE-containing and Rev-containing constructs, the
722 degree of GFP expression relative to BFP expression is proportional to the functional
723 activity of the tested Rev-RRE pair (Jackson et al., manuscript in preparation).

724 Except as noted, transfections were performed using the polyethylenamine
725 method and 8×10^5 293T/17 cells in each well of a 12-well plate. Cells were maintained
726 in 1 mL IMDM supplemented with 5% bovine calf serum. Each RRE-containing
727 construct was tested individually with the SC3 Rev-containing construct. Additionally,
728 each RRE-containing construct was transfected into cells without the addition of Rev to
729 ensure that GFP expression in this system was truly Rev-dependent. In transfections
730 performed without the Rev-containing construct, an empty CMV construct was used to

731 compensate such that each transfection was performed with a constant mass of
732 plasmid. For each transfection, 1000 ng of an RRE-containing construct and 100 ng of
733 either the MSCV-Rev construct or empty vector was used. Simultaneously, different
734 cultures of 293T/17 cells were transfected with constructs expressing GFP, BFP, or
735 mCherry alone as single-color controls to permit color compensation during flow
736 cytometry. Each set of transfections was performed in duplicate with the exception of
737 V09-2 and V13-1, for which four replicates were performed. After transfection, cells
738 were incubated for 48 h, then suspended in phosphate buffered saline. Flow cytometry
739 was performed on the resulting suspension using an Attune NxT flow cytometer with
740 autosampler attachment (Thermo Fischer Scientific). Data acquisition was performed on
741 the Attune NxT software package using the following channels:

742

Laser line	488	405	561
Emission filter	530/30	440/50	620/15
Fluorescent protein	eGFP	TagBFP	mCherry

743

744 Post-acquisition color compensation and data analysis was performed using
745 FlowJo v10 (FlowJo, LLC). For each analysis, gating was performed on single 293T/17
746 cells. Next, a daughter population of cells that expressed the RRE-containing transcript
747 was identified by gating on positivity for GFP or BFP. Using this population, the ratio of
748 arithmetic mean fluorescent intensity (MFI) of eGFP to TagBFP for successfully
749 transfected cells was calculated in both the presence and the absence of Rev. A low

750 ratio in the absence of Rev and a high ratio in its presence indicated that GFP
751 expression was Rev-dependent.

752 After determining that the RRE-containing constructs expressed GFP in a Rev-
753 dependent fashion, an additional analysis was performed to determine the functional
754 activity of specific Rev-RRE pairs. In this further analysis, only those transfections
755 including both an RRE-containing construct and the Rev-containing construct were
756 considered. An additional daughter population was created from that described above
757 by gating on mCherry positivity. This final population consisted only of single 293T/17
758 cells expressing GFP and/or BFP and also mCherry. This pattern of expression ensured
759 that selected cells were successfully co-transfected with both plasmid constructs. Once
760 this population was defined, the ratio of GFP to BFP MFI was re-calculated. This final
761 GFP:BFP ratio was used to determine the relative functional activity of different RREs
762 assessed in the presence of SC3 Rev. Differences in functional activity values between
763 RREs were evaluated using SPSS Statistics v25 (IBM). P-values were calculated using
764 a two-tailed one-way ANOVA with Tukey's HSD test for Figures 4 and 7 and with a one-
765 tailed one-way ANOVA with Dunnett's test for Figure 6E.

766 Analysis of the V08-1, V10-2, and V20-1 RREs described in Figure 4 was
767 performed with minor modifications. For this analysis, Rev was provided *in trans* by the
768 CMV-SC3 Rev construct. Each well of a 12-well plate was seeded with 4×10^5 293T/17
769 cells maintained in 2 mL IMDM supplemented with 10% bovine calf serum. One day
770 after plating, medium was removed from each well and replaced with 1 mL IMDM
771 supplemented with 5% bovine calf serum. Cells in each well were then transfected with
772 1000 ng of an RRE-containing construct and 50 ng of the CMV-Rev construct using the

773 polyethylenamine method. Four transfection replicates were performed. Simultaneously,
774 different cultures of 293T/17 cells were transfected with constructs expressing GFP or
775 BFP alone as single-color controls to permit color compensation during flow cytometry.
776 Cells were harvested and flow cytometry was performed 24 hours after transfection.
777 Gating was performed as above identifying cells successfully transduced with the RRE-
778 containing construct and expressing GFP or BFP, and the ratio of GFP:BFP was
779 calculated. Additional gating on mCherry positive cells was not performed.

780

781 **CE-SHAPE.**

782 RNA was folded as in the gel migration assay except that the final volume of the
783 folded RNA mix was 150 μ l and glycerol was excluded from the folding buffer. Folded
784 RNAs were probed using 3 mM NMIA. For this, RNAs were divided into experimental
785 (NMIA+) and control (NMIA-) aliquots (72 μ l each), to which 8 μ l 30 mM NMIA in
786 anhydrous DMSO or DMSO alone was added, respectively. Modification reactions were
787 incubated at 37°C for 50 min, ethanol precipitated, and re-suspended in 13 μ l nuclease-
788 free water. Reverse transcription of modified RNAs, cDNA processing/fractionation, and
789 SHAPE data analysis were conducted as previously described (63).

790

791 **Creating probability pairing and Shannon entropy profiles.**

792 Pairing probability (Figure S5-S8) and Shannon entropy values were calculated
793 by feeding SuperFold (49) with the 1M7 reactivities of the RREs. Shannon entropy
794 measurements were calculated over a centered 11-nt sliding window and plotted
795 against nucleotide position.

796

797 **Nucleotide sequence accession numbers.**

798 Nucleotide sequences generated through the procedure above corresponding to
799 RREs from viral quasispecies found in samples from patient SC3 were deposited in
800 Genbank under accession numbers MK190736 through MK190867. The SC3 Rev
801 sequence used in the functional assays was previously deposited under accession
802 number KF559146. The RRE sequences listed here as V10-2 and V20-1 were
803 previously deposited under accession numbers KF559160 and KF559162, respectively.

804

805 **ACKNOWLEDGMENTS**

806 This work was supported by grants GM 110009, AI134208, AI087505 and
807 AI068501 as well as the Women's Interagency HIV Study (WIHS) grant UO1-AI-35004
808 from the National Institutes of Health (NIH). The patient samples used in this manuscript
809 were collected by the Women's Interagency HIV Study (WIHS). The Bronx WHIS
810 repository provided the initial patient materials and the WIHS central repository provided
811 the materials from the intermediate time points (Bronx WIHS [Kathryn Anastos and
812 Anjali Sharma], U01-AI-035004). Jason W Rausch (NCI) is acknowledged for his
813 contribution in setting up the SHAPE-MaP analysis pipeline. S.L.G. and C.S. were
814 supported by the Intramural Research Program of the National Cancer Institute,
815 National Institutes of Health, Department of Health and Human Services. P. E. H. J. was
816 supported by grant K08AI136671 from the National Institutes of Health. Salary support
817 for M.-L.H. and D.R. was provided by the Charles H. Ross, Jr., and Myles H. Thaler
818 Endowments at the University of Virginia. The contents of this publication are solely the

819 responsibility of the authors and do not represent the official views of NIH or the WIHS.
820 The funders had no role in study design, data collection and interpretation, or the
821 decision to submit the work for publication.

822

823 **REFERENCES**

- 824 1. Rekosh D, Hammarskjold ML. 2018. Intron retention in viruses and cellular
825 genes: Detention, border controls and passports. *Wiley Interdiscip Rev RNA*
826 9:e1470.
- 827 2. Leblanc J, Weil J, Beemon K. 2013. Posttranscriptional regulation of retroviral
828 gene expression: primary RNA transcripts play three roles as pre-mRNA, mRNA,
829 and genomic RNA. *Wiley Interdiscip Rev RNA* 4:567-80.
- 830 3. Fernandes JD, Booth DS, Frankel AD. 2016. A structurally plastic
831 ribonucleoprotein complex mediates post-transcriptional gene regulation in HIV-
832 1. *Wiley Interdiscip Rev RNA* doi:10.1002/wrna.1342.
- 833 4. Hammarskjold ML, Heimer J, Hammarskjold B, Sangwan I, Albert L, Rekosh D.
834 1989. Regulation of human immunodeficiency virus env expression by the rev
835 gene product. *J Virol* 63:1959-66.
- 836 5. Hadzopoulou-Cladaras M, Felber BK, Cladaras C, Athanassopoulos A, Tse A,
837 Pavlakis GN. 1989. The rev (trs/art) protein of human immunodeficiency virus
838 type 1 affects viral mRNA and protein expression via a cis-acting sequence in the
839 env region. *J Virol* 63:1265-74.

- 840 6. Malim MH, Hauber J, Le SY, Maizel JV, Cullen BR. 1989. The HIV-1 rev trans-
841 activator acts through a structured target sequence to activate nuclear export of
842 unspliced viral mRNA. *Nature* 338:254-7.
- 843 7. Berger J, Aepinus C, Dobrovnik M, Fleckenstein B, Hauber J, Bohnlein E. 1991.
844 Mutational analysis of functional domains in the HIV-1 Rev trans-regulatory
845 protein. *Virology* 183:630-5.
- 846 8. Cochrane AW, Perkins A, Rosen CA. 1990. Identification of sequences important
847 in the nucleolar localization of human immunodeficiency virus Rev: relevance of
848 nucleolar localization to function. *J Virol* 64:881-5.
- 849 9. Kubota S, Nosaka T, Cullen BR, Maki M, Hatanaka M. 1991. Effects of chimeric
850 mutants of human immunodeficiency virus type 1 Rev and human T-cell
851 leukemia virus type I Rex on nucleolar targeting signals. *J Virol* 65:2452-6.
- 852 10. Dundr M, Leno GH, Hammarskjold ML, Rekosh D, Helga-Maria C, Olson MO.
853 1995. The roles of nucleolar structure and function in the subcellular location of
854 the HIV-1 Rev protein. *J Cell Sci* 108 (Pt 8):2811-23.
- 855 11. Kjems J, Frankel AD, Sharp PA. 1991. Specific regulation of mRNA splicing in
856 vitro by a peptide from HIV-1 Rev. *Cell* 67:169-78.
- 857 12. Battiste JL, Mao H, Rao NS, Tan R, Muhandiram DR, Kay LE, Frankel AD,
858 Williamson JR. 1996. Alpha helix-RNA major groove recognition in an HIV-1 rev
859 peptide-RRE RNA complex. *Science* 273:1547-51.
- 860 13. Daugherty MD, Liu B, Frankel AD. 2010. Structural basis for cooperative RNA
861 binding and export complex assembly by HIV Rev. *Nat Struct Mol Biol* 17:1337-
862 42.

- 863 14. Thomas SL, Oft M, Jaksche H, Casari G, Heger P, Dobrovnik M, Bevec D,
864 Hauber J. 1998. Functional analysis of the human immunodeficiency virus type 1
865 Rev protein oligomerization interface. *J Virol* 72:2935-44.
- 866 15. Booth DS, Cheng Y, Frankel AD. 2014. The export receptor Crm1 forms a dimer
867 to promote nuclear export of HIV RNA. *Elife* 3.
- 868 16. Wen W, Meinkoth JL, Tsien RY, Taylor SS. 1995. Identification of a signal for
869 rapid export of proteins from the nucleus. *Cell* 82:463-473.
- 870 17. Fischer U, Huber J, Boelens WC, Mattaj IW, Luhrmann R. 1995. The HIV-1 Rev
871 activation domain is a nuclear export signal that accesses an export pathway
872 used by specific cellular RNAs. *Cell* 82:475-483.
- 873 18. Mann DA, Mikaelian I, Zimmel RW, Green SM, Lowe AD, Kimura T, Singh M,
874 Butler PJ, Gait MJ, Karn J. 1994. A molecular rheostat. Co-operative rev binding
875 to stem I of the rev-response element modulates human immunodeficiency virus
876 type-1 late gene expression. *J Mol Biol* 241:193-207.
- 877 19. Dayton ET, Powell DM, Dayton AI. 1989. Functional analysis of CAR, the target
878 sequence for the Rev protein of HIV-1. *Science* 246:1625-9.
- 879 20. Kjems J, Brown M, Chang DD, Sharp PA. 1991. Structural analysis of the
880 interaction between the human immunodeficiency virus Rev protein and the Rev
881 response element. *Proc Natl Acad Sci U S A* 88:683-7.
- 882 21. Sherpa C, Rausch JW, Le Grice SF, Hammarskjold ML, Rekosh D. 2015. The
883 HIV-1 Rev response element (RRE) adopts alternative conformations that
884 promote different rates of virus replication. *Nucleic Acids Res* 43:4676-86.

- 885 22. Bai Y, Tambe A, Zhou K, Doudna JA. 2014. RNA-guided assembly of Rev-RRE
886 nuclear export complexes. *Elife* 3:e03656.
- 887 23. Watts JM, Dang KK, Gorelick RJ, Leonard CW, Bess JW, Jr., Swanstrom R,
888 Burch CL, Weeks KM. 2009. Architecture and secondary structure of an entire
889 HIV-1 RNA genome. *Nature* 460:711-6.
- 890 24. Cook KS, Fisk GJ, Hauber J, Usman N, Daly TJ, Rusche JR. 1991.
891 Characterization of HIV-1 REV protein: binding stoichiometry and minimal RNA
892 substrate. *Nucleic Acids Res* 19:1577-83.
- 893 25. Daly TJ, Rennert P, Lynch P, Barry JK, Dundas M, Rusche JR, Doten RC, Auer
894 M, Farrington GK. 1993. Perturbation of the carboxy terminus of HIV-1 rev affects
895 multimerization on the rev responsive element. *Biochemistry* 32:8945-8954.
- 896 26. Malim MH, McCarn DF, Tiley LS, Cullen BR. 1991. Mutational definition of the
897 human immunodeficiency virus type 1 Rev activation domain. *J Virol* 65:4248-54.
- 898 27. Heaphy S, Finch JT, Gait MJ, Karn J, Singh M. 1991. Human immunodeficiency
899 virus type 1 regulator of virion expression, rev, forms nucleoprotein filaments
900 after binding to a purine-rich "bubble" located within the rev-responsive region of
901 viral mRNAs. *Proc Natl Acad Sci U S A* 88:7366-70.
- 902 28. Zapp ML, Hope TJ, Parslow TG, Green MR. 1991. Oligomerization and RNA
903 binding domains of the type 1 human immunodeficiency virus Rev protein: a dual
904 function for an arginine- rich binding motif. *Proc Natl Acad Sci U S A* 88:7734-
905 7748.

- 906 29. Zimmel RW, Kelley AC, Karn J, Butler PJ. 1996. Flexible regions of RNA
907 structure facilitate co-operative Rev assembly on the Rev-response element. *J*
908 *Mol Biol* 258:763-77.
- 909 30. Daugherty MD, D'Orso I, Frankel AD. 2008. A solution to limited genomic
910 capacity: using adaptable binding surfaces to assemble the functional HIV Rev
911 oligomer on RNA. *Mol Cell* 31:824-34.
- 912 31. DiMattia MA, Watts NR, Stahl SJ, Rader C, Wingfield PT, Stuart DI, Steven AC,
913 Grimes JM. 2010. Implications of the HIV-1 Rev dimer structure at 3.2 Å
914 resolution for multimeric binding to the Rev response element. *Proc Natl Acad*
915 *Sci U S A* 107:5810-4.
- 916 32. Jain C, Belasco JG. 2001. Structural model for the cooperative assembly of HIV-
917 1 Rev multimers on the RRE as deduced from analysis of assembly-defective
918 mutants. *Mol Cell* 7:603-14.
- 919 33. Fornerod M, Ohno M, Yoshida M, Mattaj IW. 1997. CRM1 is an export receptor
920 for leucine-rich nuclear export signals. *Cell* 90:1051-60.
- 921 34. Otero GC, Harris ME, Donello JE, Hope TJ. 1998. Leptomycin B inhibits equine
922 infectious anemia virus Rev and feline immunodeficiency virus rev function but
923 not the function of the hepatitis B virus posttranscriptional regulatory element. *J*
924 *Virology* 72:7593-7.
- 925 35. Jackson PE, Tebit DM, Rekosh D, Hammarskjöld ML. 2016. Rev-RRE Functional
926 Activity Differs Substantially Among Primary HIV-1 Isolates. *AIDS Res Hum*
927 *Retroviruses* 32:923-34.

- 928 36. Phuphuakrat A, Paris RM, Nittayaphan S, Louisirirotchanakul S, Auewarakul P.
929 2005. Functional variation of HIV-1 Rev Response Element in a longitudinally
930 studied cohort. *J Med Virol* 75:367-73.
- 931 37. Iversen AK, Shpaer EG, Rodrigo AG, Hirsch MS, Walker BD, Sheppard HW,
932 Merigan TC, Mullins JI. 1995. Persistence of attenuated rev genes in a human
933 immunodeficiency virus type 1-infected asymptomatic individual. *J Virol* 69:5743-
934 53.
- 935 38. Churchill MJ, Chiavaroli L, Wesselingh SL, Gorry PR. 2007. Persistence of
936 attenuated HIV-1 rev alleles in an epidemiologically linked cohort of long-term
937 survivors infected with nef-deleted virus. *Retrovirology* 4:43.
- 938 39. Bobbitt KR, Addo MM, Altfeld M, Filzen T, Onafuwa AA, Walker BD, Collins KL.
939 2003. Rev activity determines sensitivity of HIV-1-infected primary T cells to CTL
940 killing. *Immunity* 18:289-99.
- 941 40. Baccam P, Thompson RJ, Li Y, Sparks WO, Belshan M, Dorman KS,
942 Wannemuehler Y, Oaks JL, Cornette JL, Carpenter S. 2003. Subpopulations of
943 equine infectious anemia virus Rev coexist in vivo and differ in phenotype. *J Virol*
944 77:12122-12131.
- 945 41. Belshan M, Baccam P, Oaks JL, Sponseller BA, Murphy SC, Cornette J,
946 Carpenter S. 2001. Genetic and biological variation in equine infectious anemia
947 virus Rev correlates with variable stages of clinical disease in an experimentally
948 infected pony. *Virology* 279:185-200.

- 949 42. Belshan M, Harris ME, Shoemaker AE, Hope TJ, Carpenter S. 1998. Biological
950 characterization of Rev variation in equine infectious anemia virus. *Journal of*
951 *virology* 72:4421-6.
- 952 43. Sloan EA, Kearney MF, Gray LR, Anastos K, Daar ES, Margolick J, Maldarelli F,
953 Hammarskjold ML, Rekosh D. 2013. Limited nucleotide changes in the Rev
954 response element (RRE) during HIV-1 infection alter overall Rev-RRE activity
955 and Rev multimerization. *J Virol* 87:11173-86.
- 956 44. Smola MJ, Christy TW, Inoue K, Nicholson CO, Friedersdorf M, Keene JD, Lee
957 DM, Calabrese JM, Weeks KM. 2016. SHAPE reveals transcript-wide
958 interactions, complex structural domains, and protein interactions across the Xist
959 lncRNA in living cells. *Proc Natl Acad Sci U S A* 113:10322-7.
- 960 45. Sztuba-Solinska J, Rausch JW, Smith R, Miller JT, Whitby D, Le Grice SFJ.
961 2017. Kaposi's sarcoma-associated herpesvirus polyadenylated nuclear RNA: a
962 structural scaffold for nuclear, cytoplasmic and viral proteins. *Nucleic Acids Res*
963 45:6805-6821.
- 964 46. Lu YF, Mauger DM, Goldstein DB, Urban TJ, Weeks KM, Bradrick SS. 2015.
965 IFNL3 mRNA structure is remodeled by a functional non-coding polymorphism
966 associated with hepatitis C virus clearance. *Sci Rep* 5:16037.
- 967 47. Siegfried NA, Busan S, Rice GM, Nelson JA, Weeks KM. 2014. RNA motif
968 discovery by SHAPE and mutational profiling (SHAPE-MaP). *Nat Methods*
969 11:959-65.
- 970 48. Smola MJ, Calabrese JM, Weeks KM. 2015. Detection of RNA-Protein
971 Interactions in Living Cells with SHAPE. *Biochemistry* 54:6867-75.

- 972 49. Smola MJ, Rice GM, Busan S, Siegfried NA, Weeks KM. 2015. Selective 2'-
973 hydroxyl acylation analyzed by primer extension and mutational profiling
974 (SHAPE-MaP) for direct, versatile and accurate RNA structure analysis. Nat
975 Protoc 10:1643-69.
- 976 50. Sherpa C, Rausch JW, Le Grice SFJ. 2018. Structural characterization of
977 maternally expressed gene 3 RNA reveals conserved motifs and potential sites
978 of interaction with polycomb repressive complex 2. Nucleic Acids Res
979 doi:10.1093/nar/gky722.
- 980 51. Bellaousov S, Reuter JS, Seetin MG, Mathews DH. 2013. RNAstructure: Web
981 servers for RNA secondary structure prediction and analysis. Nucleic Acids Res
982 41:W471-4.
- 983 52. Jackson PEH, Huang J, Sharma M, Rasmussen SK, Hammarskjold M-L, Rekosh
984 D. 2019. An assay to measure the activity of RNA elements and proteins that
985 promote the expression of mRNA with retained introns. bioRxiv 551846.
986 doi:<https://doi.org/10.1101/551846>.
- 987 53. Srinivasakumar N, Chazal N, Helga-Maria C, Prasad S, Hammarskjold ML,
988 Rekosh D. 1997. The effect of viral regulatory protein expression on gene
989 delivery by human immunodeficiency virus type 1 vectors produced in stable
990 packaging cell lines. J Virol 71:5841-8.
- 991 54. Deigan KE, Li TW, Mathews DH, Weeks KM. 2009. Accurate SHAPE-directed
992 RNA structure determination. Proc Natl Acad Sci U S A 106:97-102.
- 993 55. McGinnis JL, Dunkle JA, Cate JH, Weeks KM. 2012. The mechanisms of RNA
994 SHAPE chemistry. J Am Chem Soc 134:6617-24.

- 995 56. Tiley LS, Malim MH, Tewary HK, Stockley PG, Cullen BRJPotNAoS. 1992.
996 Identification of a high-affinity RNA-binding site for the human immunodeficiency
997 virus type 1 Rev protein. 89:758-762.
- 998 57. Lichinchi G, Gao S, Saletore Y, Gonzalez GM, Bansal V, Wang Y, Mason CE,
999 Rana TMJNm. 2016. Dynamics of the human and viral m 6 A RNA methylomes
1000 during HIV-1 infection of T cells. 1:16011.
- 1001 58. Palmer S, Wiegand AP, Maldarelli F, Bazmi H, Mican JM, Polis M, Dewar RL,
1002 Planta A, Liu S, Metcalf JA, Mellors JW, Coffin JM. 2003. New real-time reverse
1003 transcriptase-initiated PCR assay with single-copy sensitivity for human
1004 immunodeficiency virus type 1 RNA in plasma. J Clin Microbiol 41:4531-6.
- 1005 59. Kearney M, Maldarelli F, Shao W, Margolick JB, Daar ES, Mellors JW, Rao V,
1006 Coffin JM, Palmer S. 2009. Human immunodeficiency virus type 1 population
1007 genetics and adaptation in newly infected individuals. J Virol 83:2715-27.
- 1008 60. Magoc T, Salzberg SL. 2011. FLASH: fast length adjustment of short reads to
1009 improve genome assemblies. Bioinformatics 27:2957-63.
- 1010 61. Adachi A, Gendelman HE, Koenig S, Folks T, Willey R, Rabson A, Martin MA.
1011 1986. Production of acquired immunodeficiency syndrome-associated retrovirus
1012 in human and nonhuman cells transfected with an infectious molecular clone. J
1013 Virol 59:284-91.
- 1014 62. Shaner NC, Campbell RE, Steinbach PA, Giepmans BN, Palmer AE, Tsien RY.
1015 2004. Improved monomeric red, orange and yellow fluorescent proteins derived
1016 from *Discosoma* sp. red fluorescent protein. Nat Biotechnol 22:1567-72.

1017 63. Lusvarghi S, Sztuba-Solinska J, Purzycka KJ, Pauly GT, Rausch JW, Grice SF.
1018 2013. The HIV-2 Rev-response element: determining secondary structure and
1019 defining folding intermediates. *Nucleic Acids Res* 41:6637-49.

1020

1021 **FIGURE LEGENDS:**

1022 Figure 1: Patient SC3 HIV viral load and CD4 count at each visit during participation in
1023 the WIHS cohort. Sequential study visits occurred about six months apart and blood
1024 samples were obtained at each visit. V01 refers to the first visit, V04 to the fourth, etc.
1025 Data is missing for unattended visits. HIV sequences could first be amplified from
1026 plasma samples obtained at V08 and onwards. However, HIV seroconversion was first
1027 appreciated under the WIHS protocol at V10 and viral loads were only performed from
1028 this visit on. The patient died after V20.

1029

1030 Figure 2: Evolutionary alignment of SC3 RREs. Deep sequencing of viral RNA was
1031 performed from plasma collected at each study visit. This alignment includes RRE
1032 contigs that were present in at least 5% of the total sequences as explained in the
1033 methods. Sequence labels are in the form of VXX-Y where XX refers to visit number
1034 and Y refers to rank order of the contig within that visit plasma sample. Nucleotide
1035 changes relative to the presumptive founder sequence, V08-1, are highlighted.
1036 Mutations (Mut) 1-5 refer to single nucleotide changes that occur in V20-1 relative to
1037 V08-1. Mut 5 is highlighted in red, as this change is also found in V10-2 and was not
1038 recognized in our previous study of the “early” and “late” RREs from patient SC3 (43).

1039 (See also Figures S1 for the alignment including minority variants and S2 for the
1040 complete nucleotide sequences included here.)

1041

1042 Figure 3: Structures of selected SC3 RREs. Secondary structures of [A] V08-1, [B] V10-
1043 2, [C] V09-2, and [D] V20-1 234-nt RREs were determined by SHAPE-MaP. 1M7
1044 reactivities of RRE nucleotides are color coded and superimposed on the structures.
1045 The positions of the mut 1, mut 2, mut 3, and mut 4 single nucleotide changes are
1046 represented by black arrows. Green labelled arrows show where the nucleotide at this
1047 position varies from V08-1, the presumptive founder sequence, and V10-2. In V09-2,
1048 the mut 3 position shows a G to A change, while the mut 3 position in V20-1 shows a G
1049 to C change. The mut 5 position is shown with a red arrow and is additionally labelled
1050 with “mut 5” in structures where the nucleotide varies from V08-1. [E] Migration of V10-2
1051 and V20-1 RRE on a native PAGE gel was visualized after 22 hours by UV shadowing.

1052

1053 Figure 4: Functional activity of SC3 founder (V08-1), “early” (V10-2), and “late” (V20-1)
1054 RREs. Functional activity of the three RREs was determined by transfecting reporter
1055 constructs containing the different RREs into 293T/17 cells along with 50 ng of SC3 Rev
1056 and measuring the ratio of the mean fluorescent intensity of GFP to BFP. $N=4$, SEM is
1057 represented by error bars. P-values of <0.05 are represented by *, NS=non-significant
1058 difference.

1059

1060 Figure 5: Secondary structures of full-length (351-nt) V10-2 and V20-1 SC3 RREs.
1061 Secondary structures of [A] V10-2 and [B] V20-1 SC3 RREs, determined by CE-

1062 SHAPE. NMIA nucleotide reactivities are color coded and superimposed on the
1063 structures. The positions of the eight nucleotides differing between the two RREs are
1064 represented by arrows. Mutations within the short 234-nt RRE are designated mut 1,
1065 mut 2, mut 3, and mut 4 and shown in green on the V20-1 RRE. Four additional
1066 mutations within stem SL-I are shown as green arrows without labels on the V20-1
1067 RRE. The position of each of these changes is shown by black arrows on the V10-2
1068 RRE.

1069

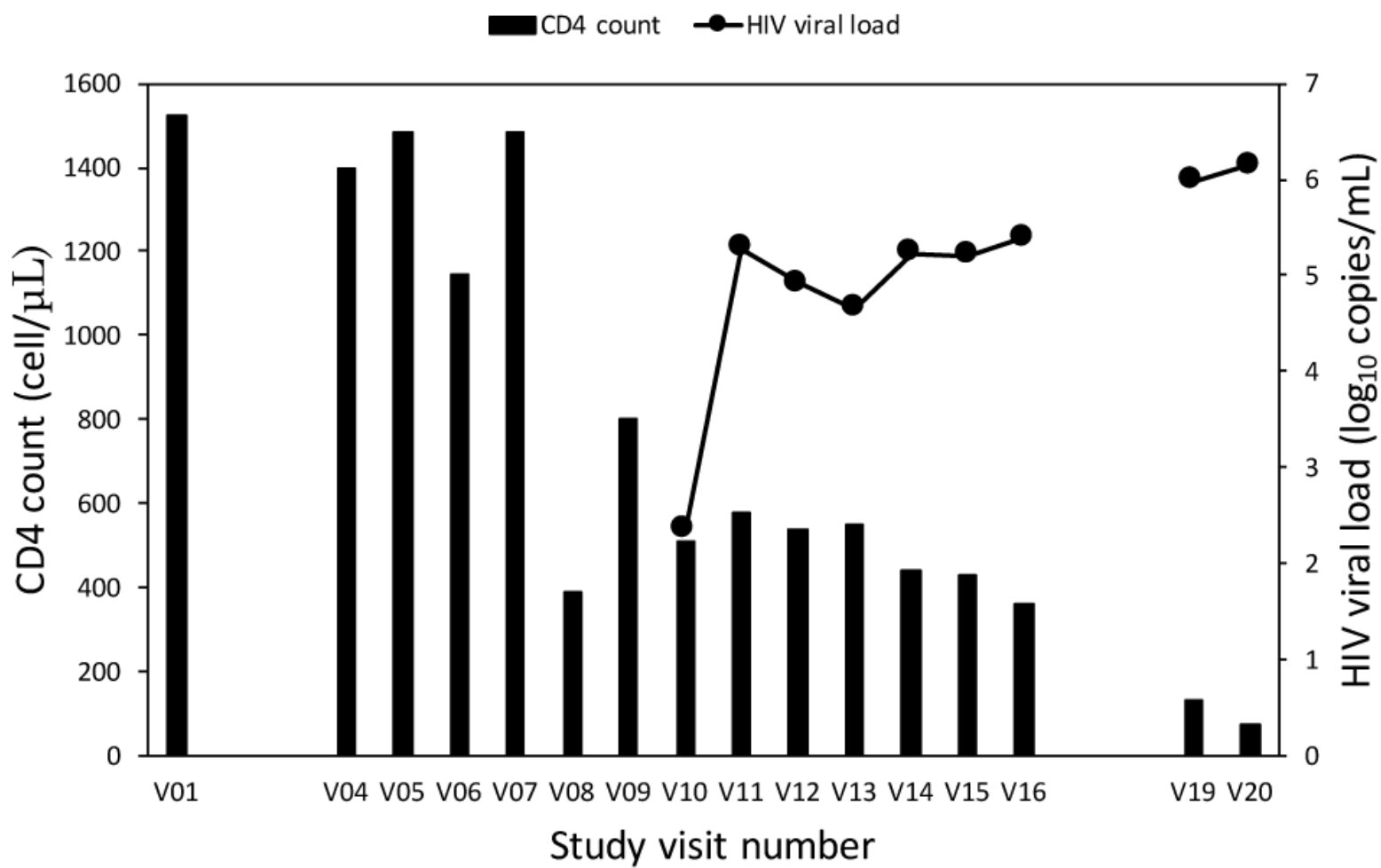
1070 Figure 6: Secondary structures and function of V10-2 RRE single mutants. Secondary
1071 structures of the [A] M1, [B] M2, [C] M3, and [D] M4 SC3 RREs were determined by
1072 SHAPE-MaP. 1M7 reactivities are color coded and superimposed on the structures. The
1073 positions of mut 1-5 are represented by black and green arrows. Mut 1, mut 2, mut 3,
1074 and mut 4 are indicated in green on the RREs where the nucleotide at that position
1075 differs from V10-2, while mut 5 is represented in red and is present on every structure.
1076 [E] Rev-RRE functional activity of M1-M4 RREs compared with V10-2 and V20-1 in the
1077 presence of 100 ng SC3 Rev. N=2, SEM are represented by error bars. Selected p-
1078 values of <0.05 and <0.001 are represented by * and ***, respectively.

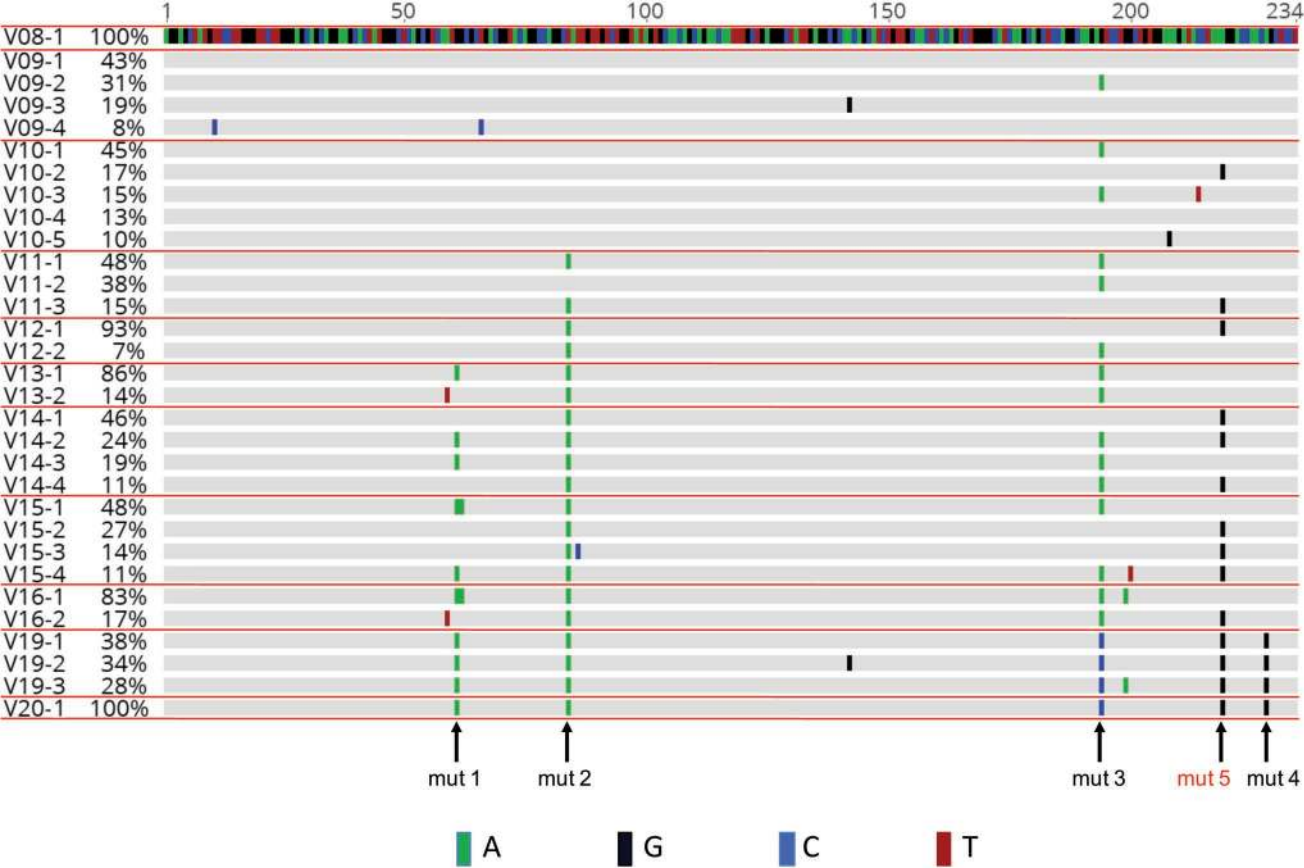
1079

1080 Figure 7: Rev-RRE activity of SC3 RRE haplotypes. Activity of selected RREs was
1081 determined in the presence of 100 ng Rev using the fluorescent assay system. N=2
1082 except for V9-2 and V13-1 where N=4. SEM are represented by the error bars. Selected
1083 p-values of <0.05 and <0.001 are represented by * and ***, respectively.

1084

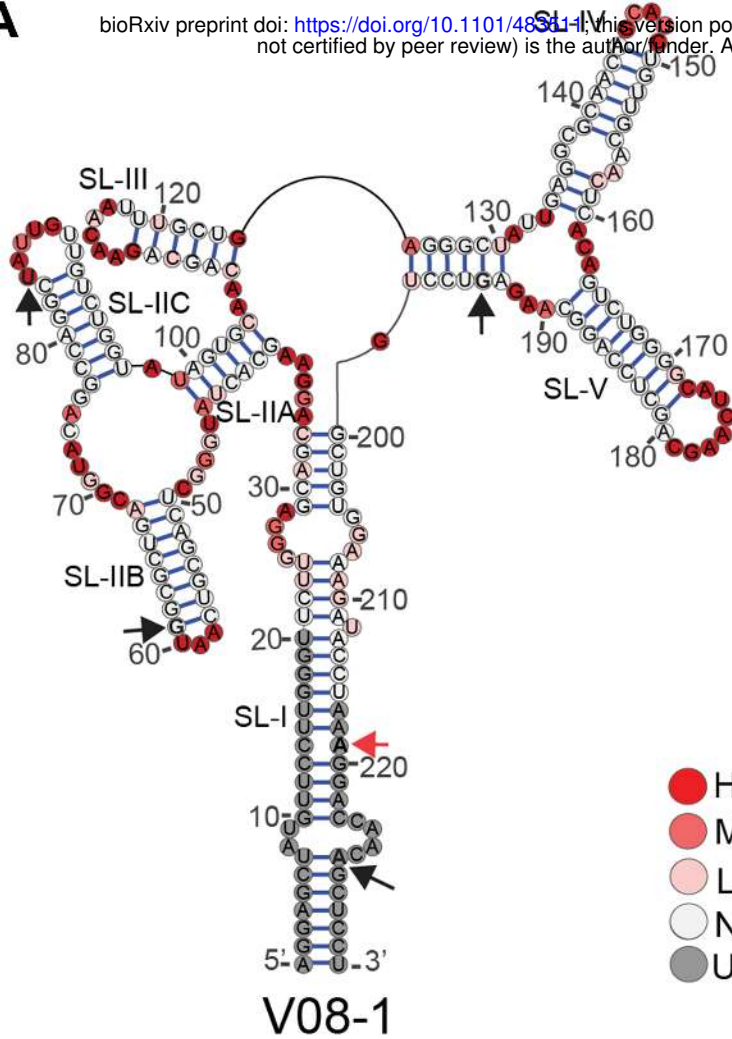
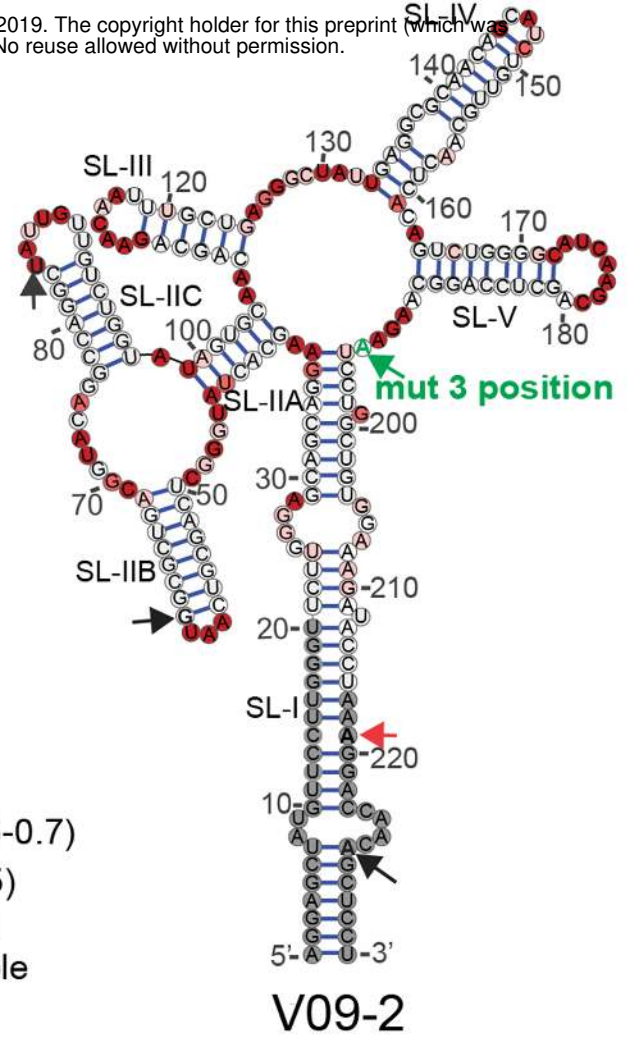
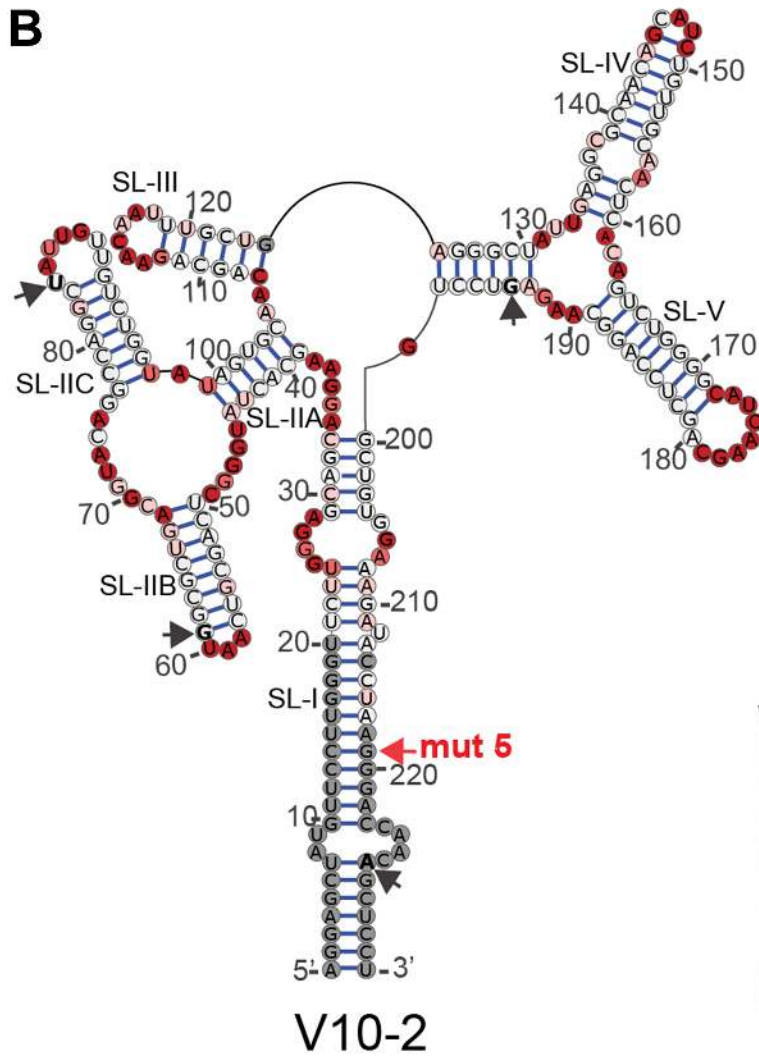
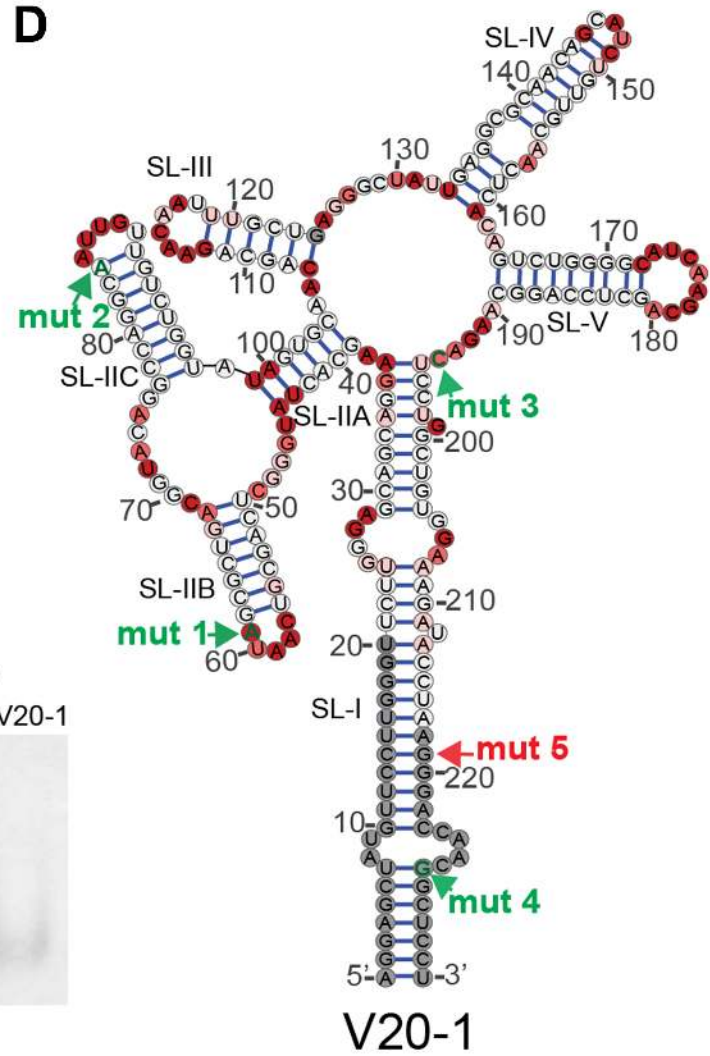
1085 Figure 8: Shannon entropy profiles of SC3 RRE variants and single mutants. Shannon
1086 entropy values of the SHAPE-MaP generated RRE structures, smoothed over centered
1087 11-nt sliding windows are plotted as a function of nucleotide position. Higher Shannon
1088 entropy suggests regions that are structurally dynamic. The boxed regions correspond
1089 to the loop between SL-IIA and SL-IIB (Region I) and the loop between SL-IIB and SL-
1090 IIC (Region II). These regions display high Shannon entropy in the high-activity V20-1
1091 structure and low entropy in the lower activity V08-1 structure.





A

bioRxiv preprint doi: <https://doi.org/10.1101/483111>; this version posted February 15, 2019. The copyright holder for this preprint (which was not certified by peer review) is the author/funder. All rights reserved. No reuse allowed without permission.

**C****B****D****E**

